

Near-Field Focused Reflectarray Antenna and Reconfigurable Intelligent Surfaces: The Potential of Wave Propagation Control for Smart Radio Environment

Wael Elshennawy*

Abstract—Reconfigurable intelligent surfaces (RISs) have recently attracted attention in the implementation of smart radio environment. In this paper, RISs are realized by the near-field focused antennas (NFF). A near-field channel gain model of RIS-assisted wireless communications is developed for an NFF reflectarray antenna based on the physics and electromagnetic nature of the RISs. The developed model entails the computation of the reflectarray aperture efficiency. Also, it takes into account reflectarray reconfigurability to cope with varying environment, physical factors like the physical dimensions of the RISs, and the radiation patterns of the unit cells. Moreover, it is characterised by a reduction in the complexity. This model is further used in computing the positioning performance bounds and estimating the RIS optimal beamformer weights. For a validation purpose, the model is simulated by using Matlab software, and the results are compared to the simulation results of a near-field model discussed in literature. The comparison shows a very good agreement. Finally, the reflectarray antenna is thinned to achieve a performance comparable to a fully populated reflectarray antenna case using the full wave 3D electromagnetic solver CST Microwave Studio (CST MWS).

1. INTRODUCTION

Future wireless networks are expected to evolve toward intelligent and software reconfigurable paradigms enabling ubiquitous communications between humans and mobile devices [1]. They will be capable of sensing, controlling, and optimizing the wireless environment to fulfill the visions of low-power, high-throughput, massively-connected, and low-latency communications [2]. A key conceptual enabler that is recently gaining increasing popularity is the RIS, which represents a breakthrough technology. RIS is rapidly evolving to support the software-defined networking (SDN) [3]. RISs can effectively re-engineer impinging electromagnetic waves in a controlled manner and provide different functions including steering toward any direction, full absorption, polarization manipulation, and more. Therefore, RISs can bring benefits to the wireless communications [4], multiple inputs multiple outputs (MIMO) broadcasting for simultaneous wireless information and power transfer [5], secure transmission [6], backscatter communications [7], and localization and positioning [8].

RISs and NFF arrays share common functions of electromagnetic waves manipulation such as the control of sidelobe level, -3 dB focal spot, implement multifocus NFF antennas, and electronically scan the focal point [9]. Thus, there is a growing interest in the application of NFF RISs, which highly concentrate the electromagnetic (EM) power into small spot regions in smart radio environment [1]. This feature of NFF RISs goes beyond the beam-steering capability by focusing the radiated field over a constrained field of view (FoV). So, they can simultaneously control the direction of the radiated wavefront and the depth of focus [2]. This high focusing capability can serve multiple applications, i.e.,

Received 3 December 2020, Accepted 7 January 2021, Scheduled 18 January 2021

* Corresponding author: Wael Elshennawy (wael.elshennawy@orange.com).

The author is with the Orange Business Services Co., Cairo, Egypt.

making possible the precise radio localization of users [10], mapping of environments [11], etc. NFF RISs can be implemented by a number of different technologies and layouts [12]. Most notably, technologies that allow for the implementation of planar NFF antennas are preferred, especially array antennas. The phase of each antenna element current is adjusted to achieve constructive interference of all field contributions at the focal point [9].

The limitation associated with RIS-assisted wireless communications operating in the near-field is the lack of reliable electromagnetic models for the RISs. Majority of the existing research works are based on far-field models [13, 14]. Therefore, it may lead to relatively simplified algorithm designs and performance predictions [15]. The path loss models used in most existing works do not consider physical factors such as the size of the RISs, nor the dimensions of the antenna elements [14]. Channel models play an important role in assessing the performance of modulation, equalization, and coding techniques on real channels. Moreover, the channel gain models describe the near-field scattering problem, which usually involves high complexity burden accompanied by an evaluation of multiple integration equations [16–18]. To this end, the need of developing a near-field channel gain model is characterized as a low complexity and a simple electromagnetic model. Besides, the accuracy of estimating the positioning and localization primarily depends on reliable channel gain model to cope with the dynamic changes in the smart radio environment.

In this paper, NFF RIS is employed to support only two electromagnetic waves manipulation functions, i.e., steer and focus in the near-field region. NFF RIS is realized by using a reflectarray antenna. A near-field model for the computation of the reflectarray antenna channel gain is developed, which takes into account many factors like the physical dimension of the RISs, dimensions of the unit cells, and the radiation pattern of the unit cells. This model encompasses the calculation of reflectarray antenna aperture efficiency and takes into account the elements dimensions reconfigurability in computing the channel gain. The complexity of calculating the near-field scattered fields is merely reduced into an operation of searching the Fresnel integral tables instead of computing the integration equations of the EM scattering problem [17, 18]. The model is validated by comparing its simulation results with a near-field model discussed in [19] by using Matlab software. Then the model is exploited in the near-field phase-only synthesis (POS) technique to compute the optimal RIS beamformer weights. A Fisher information matrix (FIM) analysis is discussed for NFF RIS, and FIM is used to derive the position error bounds (PEB). Finally, the reflectarray antenna is thinned with the aim of obtaining fewer reflectarray antenna elements by using a CST MWS, that achieves the required target focus area without causing major degradation in NFF RIS radiation pattern characteristics.

2. SYSTEM MODEL

2.1. Geometry Model

An RIS-aided communication for 3D setup is shown in Figure 1 where an offset-feed antenna source, e.g., base station (BS), transmits a signal received by an RIS. Then, it scatters back toward a single-antenna receiver, e.g., user equipment (UE). An RIS is located in the x - y plane at \mathbf{x}_k . The RIS is modeled as a reflectarray antenna with inter-element spacing $\lambda/2$ to avoid the mutual coupling effect, where λ denotes the signal wavelength. The reflectarray antenna elements $m \in \{1, \dots, M\}$ are arranged periodically along x and y coordinates with an edge boundary. The BS is located in the xz -plane at \mathbf{x}_{BS} with a distance l_0 from the center of the RIS and an angle $\theta_0 \in [0, \pi/2]$. It transmits a \mathbf{y} -co-polarized wave toward the RIS with its radiation boresight pointing toward the reflectarray antenna center. It scatters off the RIS and travels toward the UE at a distance d from the center of the RIS and an angle $\varphi \in [-\pi/2, \pi/2]$. The UE can span the entire plane, and its unknown location parameter is \mathbf{x} . BS and UE are synchronized. The RIS is intelligent in the sense that the m -reflecting elements can adaptively change their phases in order to spatially steer a main beam toward the UE.

2.2. Signal and Channel Model

The received complex baseband signal at the UE is composed of a scattered signal as in [20]

$$\mathbf{y}(t) = \alpha s(t - \tau) + w(t), \quad (1)$$

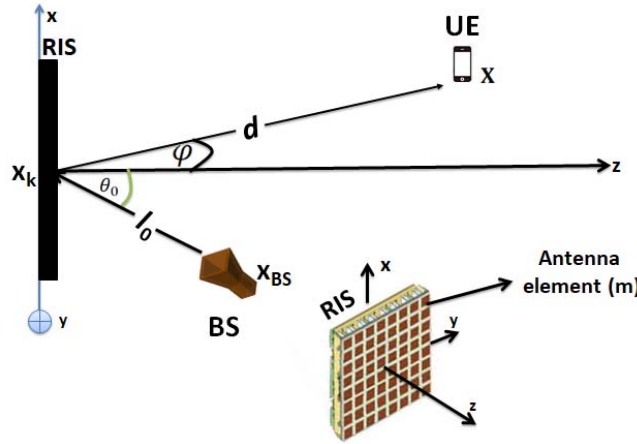


Figure 1. Graphical illustration for the scenario that is used in the problem formulation. Near-field focused reflectarray antenna with M elements. The reflectarray is illuminated by a rectangular feed horn antenna.

where α is the channel gain, $s(t)$ a known orthogonal frequency division multiplexing (OFDM) signal with an average transmit power P at a carrier frequency f_c , and $w(t)$ a white Gaussian noise with power spectral density (PSD) $N_0/2$. $\tau = \|\mathbf{x}_k - \mathbf{x}_{BS}\|/c + \|\mathbf{x} - \mathbf{x}_k\|/c$, and c denotes the speed of light. The paper discusses the case of narrowband near-field operation mode, where the condition $\max(\|\mathbf{x}_k - \mathbf{x}_{BS}\|, \|\mathbf{x} - \mathbf{x}_k\|) \leq 2D^2/\lambda$ is satisfied, and D is the largest reflectarray antenna dimension. The signals at the reflectarray antenna elements are not resolvable in the delay domain. The channel gains from the BS to an RIS h_m and from an RIS to the UE g_m are expressed as

$$h_m = \rho_m^{BR} e^{j\phi_m^{BR}}, \tag{2}$$

$$g_m = \rho_m^{RU} e^{j\phi_m^{RU}}. \tag{3}$$

ρ_m^{BR} , ρ_m^{RU} , ϕ_m^{BR} , ϕ_m^{RU} are the magnitudes and phases of the complex channel gains. The phases can be expressed as

$$e^{j\phi_m^{BR}} = e^{-j2\pi\|\mathbf{x}_{BS}-\mathbf{q}_m\|/\lambda}, \tag{4}$$

$$e^{j\phi_m^{RU}} = e^{-j2\pi\|\mathbf{x}-\mathbf{q}_m\|/\lambda}, \tag{5}$$

where $\mathbf{q}_m = (x_m, y_m, 0)$ is the position of the reflectarray antenna unit cell.

2.3. Problem Formulation

NFF RIS can improve the spatial resolution of a localization system [9]. The most evident design criterion consists of exploiting the well-known optical focusing concept by achieving a constructive in-phase summation, i.e., focal point at the target point [9]. In smart-radio environment, the UE moves from a location to another, which requires the use of near-field model exhibiting low complexity for computing the channel gain in response to the dynamic smart radio environment changes. Thus, this allows to rapidly change the antenna geometrical configuration of NFF RIS to acquire the proper phase distribution of the radiation currents on the aperture surface. The required reflectarray antenna excitation profile here will be derived from the phase-conjugate approach.

3. NEAR-FIELD CHANNEL GAIN ANALYSIS

3.1. RIS Signal Model

The observed signal at the antenna UE, subcarrier $n \in \{0, \dots, N-1\}$, and time $t \in \{1, \dots, T\}$ is expressed as

$$y_{n,t} = \mathbf{h}^T \mathbf{\Omega} \mathbf{g}_{s_{n,t}} e^{-j2n\Delta_f \tau/c} + w_{n,t}, \tag{6}$$

where ($\Upsilon = \frac{1}{2}\sqrt{Z_0}E_0^2A$) is the total power radiated by the antenna aperture size area A ; Z_0 is the intrinsic impedance of free space; and E_0 is the aperture field amplitude. $P_r = z^2|\overline{S}|$ is the power radiated by unit solid angle in the z direction, and \overline{S} is the Poynting vector. The discussion will be only restricted to a plane structure, and the analysis will be based on the scalar field theory [24]. Thus, it is assumed that the field over the aperture is uniformly polarized in one direction. The field distribution over the aperture will be designated by Π , which is defined as a product of the amplitude distribution Λ and the phase distribution B as follows.

$$\Pi = \Lambda e^{-jB}. \tag{11}$$

It is convenient to change the notations somewhat from those used in Equations (10), (11) for the next two subsections.

1) *BS to RIS*: For the case of propagation emanating from the BS toward the reflectarray antenna in the focal plane near the axis, the electric field of a focused aperture has all the properties of the Fraunhofer region in complete agreement with the Fresnel fields expression given in [23]. This is as well asserted by Silver for the field on the axis in the Fresnel region in [24]. Therefore, the field impinging on the reflectarray antenna elements by the feed antenna can be expressed as [9].

$$E_m^{\text{BR}} = \Lambda_m^{\text{BR}} e^{jv_{m,f}} = F(\hat{r}_{m,f}) \frac{e^{-jkl_m}}{l_m}, \tag{12}$$

$$F(\hat{r}_{m,f}) = A_f e^{j\phi_f} (\cos \theta_{m,f})^q; \quad (0 \leq \theta_{m,f} \leq \pi/2), \tag{13}$$

where (r_f, θ_f, ϕ_f) represent the feed antenna spherical coordinates; A_f is the complex amplitude, $\hat{r}_{m,f}$ is the unit vector pointing from the feed antenna toward the reflectarray antenna element; and $\theta_{m,f}$ is the angle between $\hat{r}_{m,f}$ and the normal direction to the aperture plane as illustrated in 2(b). The pattern shape of the feed's radiation is modeled by a cosine taper raised to an exponent q , whose value is determined by matching Eq. (13) with the actual feed's radiation pattern [25]. ρ_m^{BR} can be expressed as

$$\rho_m^{\text{BR}} = \sqrt{\frac{4\pi H^2 |\overline{S}_{\text{BR},m}|}{\frac{1}{2}\sqrt{Z_0}(E_{0,\text{feed}})^2 A_{\text{feed}}}}, \tag{14}$$

where H is the height of the feed antenna, $|\overline{S}_{\text{BR},m}|$ the Poynting vector directed toward reflectarray antenna m th element, $E_{0,\text{feed}}$ the feed antenna aperture field amplitude, and A_{feed} the feed antenna size area.

2) *RIS to UE*: The fields scattered by reflectarray antenna m th elements are focused into the Fresnel region. The total fields emanating by the reflectarray antenna elements at UE can be expressed in [9] as follows

$$E^{\text{RU}} = \sum_{m=1}^M e^{-j\psi_{mn}} E_m^{\text{BR}} E_{mn}. \tag{15}$$

The complexity of field calculation is simply reduced into a scalar scattering problem, where E_{mn} can be expressed as in [23]

$$\begin{aligned} E_{mn} = & \frac{z'_n u}{2} [C_{a_m, x'_n, +} + C_{a_m, x'_n, -} - jS_{a_m, x'_n, +} - jS_{a_m, x'_n, -}] \\ & [C_{b_m, y'_n, +} + C_{b_m, y'_n, -} - jS_{b_m, y'_n, +} - jS_{b_m, y'_n, -}] \\ & \frac{jE_{0,m}^{\text{RU}}}{d_m} (\cos \theta_{mn})^{qe}; \quad (0 \leq \theta_{mn} \leq \pi/2), \end{aligned} \tag{16}$$

where $E_{0,m}^{\text{RU}}$ is the reflectarray antenna m th element aperture field amplitude, and a_m and b_m are the reflectarray antenna m th element dimension in x, y coordinates, respectively. C, S , and ψ_{mn} terms are expressed in [23] as follows

$$C_{\kappa, \chi, \pm} = C \left(\frac{\kappa \pm 2u\chi}{\sqrt{z'_n u \lambda}} \right). \tag{17}$$

$$S_{\kappa,\chi,\pm} = S \left(\frac{\kappa \pm 2u\chi}{\sqrt{z'_n u \lambda}} \right). \quad (18)$$

$$\psi_{mn} = k \left[z'_n - \frac{u-1}{2z'_n} (x_n'^2) + (y_n'^2) \right]. \quad (19)$$

$u = d_0/(d_0 - z'_n)$, $(\cos \theta_{mn})^{q_e}$ is the m th reflectarray antenna element radiation pattern raised to an exponent q_e , and d is the distance from the reflectarray antenna center to the UE location $\mathbf{x} = (x'_n, y'_n, z'_n)$ as depicted in Figure 2. The integral equations of scattering problem are computed by using the tabulated Fresnel integrals in [26]. The Fresnel integrals are defined as follows:

$$C(\Sigma) = \int_0^\Sigma \cos \frac{\pi}{2} \varrho^2 d\varrho, \quad (20)$$

$$S(\Sigma) = \int_0^\Sigma \sin \frac{\pi}{2} \varrho^2 d\varrho, \quad (21)$$

where Σ takes the arguments of C and S in Equations (17) and (18). Due to the spreading term factor $e^{-j\psi_{mn}}/d_m$, the peak of the radiated field does not occur at the focal point where all field contributions sum in phase, but it is located at a point between the reflectarray antenna aperture and the focal point [9]. This remark will be further demonstrated in the next simulation results section. It is evident that this model reduces the complexity of computing scattering integral equations. The intensity of $|E_{mn}|^2$ can be computed by use of the tables in [26]. Similarly, ρ_m^{RU} can be expressed as

$$\rho_m^{\text{RU}} = \sqrt{\frac{4\pi z_n'^2 |\overline{S}_{\text{RU},m}|}{\frac{1}{2} \sqrt{Z_0} \left(\sum_m E_{0,m}^{\text{RU}} \right)^2 A_m}} \quad (22)$$

where $|\overline{S}_{\text{RU},m}|$ is the Poynting vector directed from reflectarray antenna m th element toward UE location, $E_{0,m}^{\text{RU}}$ the reflectarray antenna m th unit cell aperture field amplitude, and A_m the reflectarray antenna m th unit cell size area. It is noteworthy that the aforementioned expressions for the Fresnel fields are valid under the assumption that there is a small phase deviation between reflectarray antenna elements. Otherwise, the nonuniform phase distribution on the aperture results in highly dispersed system of rays in the target focusing area [24].

3.3. Complexity Analysis

The complexity of this model and other models [18, 27] commonly have the same number of floating-point operations (FLOPs) for an equal number of reflectarray antenna elements and the number of UE locations N' . It usually costs $\mathcal{O}(MN')$ FLOP, where FLOP refers to a single complex floating point operation, e.g., addition and multiplication. Nevertheless, the main difference inherits in the calculation of the scattered fields, which has been simplified here into an operation of searching Fresnel integral tables. The choice among the searching algorithms usually renders to their ability to cope with the dynamic environment changes. Also, the candidate searching algorithm has to be characterized by the lowest average time complexity. For instance, binary search algorithm has a complexity $\mathcal{O} \log(n_E)$, where n_E refers to the number of table entries.

The model discussed in [27] involves a division operation on each new UE location \mathbf{x} , and it costs $\mathcal{O}(M(n'') \log(n''))$, where $\mathcal{O}M(n'')$ refers to the complexity of the multiplication algorithm, and $\log(n'')$ refers to the complexity per digit numbers n'' . It is obvious that the developed channel gain model is characterized as low complexity due to the reduction in computing the scattered fields by searching the Fresnel tables instead of performing cumbersome integration operations.

3.4. Reflectarray Aperture Efficiency

The aperture efficiency of the reflectarray antenna has to be calculated for proper channel gain calculation. The aperture efficiency includes many efficiency factors that affect the aperture efficiency of the

reflectarray antenna. Among the different efficiency factors discussed in [28], two paramount terms are presented here in the context; spillover efficiency η_s and illumination efficiency η_i . $\eta_s < 1$ incurs a loss for \mathbf{h} , where it corresponds to the percentage of the radiated power from the feed antenna intercepted by the reflectarray antenna. $\eta_i < 1$ is associated with \mathbf{g} , and it corresponds to a measure of the uniformity of amplitude and phase of field distribution on the reflectarray antenna aperture. Thus, the aperture efficiency can be expressed as the product of these two terms,

$$\mu = \mu_i \mu_s. \quad (23)$$

Meanwhile, other efficiency factors are typically associated with the choice of reflectarray phasing elements [22]. A discussion on these efficiency factors and their influences on aperture efficiency is not explored in this paper. For the case of an offset-feed reflectarray antenna, the reflectarray aperture plane is illuminated by an offset feed source located at \mathbf{x}_{BS} as illustrated in Figure 2(b). The expressions for μ_s and μ_i are derived based on [25] in the framework of the channel gain formulation, and their product equals μ in Equation (8). These efficiency factors μ_s and μ_i are mathematically expressed as

$$\mu_s = \frac{(2q+1)H}{2\pi(2l_0)^{2q}} \int_0^{W'} \int_0^{L'} \frac{(l_0^2 + \zeta)^{2q}}{(x_m^2 + y_m^2 + \zeta)^{q+3/2}} dy dx. \quad (24)$$

$$\mu_i = \frac{1}{A_a} \frac{\left| \iint \frac{(l_0^2 + \zeta)^q}{(x_m^2 + y_m^2 + \zeta)^{1+q+q_e}} dx dy \right|^2}{\iint \left| \frac{(l_0^2 + \zeta)^q}{(x_m^2 + y_m^2 + \zeta)^{1+q+q_e}} \right|^2}, \quad (25)$$

where $\zeta = H^2 \sec^2 \theta_0 + y_m(2H \tan \theta_0)$. The dimensions of a rectangular reflectarray aperture are W' and L' along the x and y axes, respectively, and their size area corresponds to A_a . $\cos \theta^q$ and $\cos \theta^{q_e}$ radiation pattern models are adopted throughout the paper for simplicity purpose. Their exponents q and q_e control the antenna directivity and the shape of the pattern. For instance, as q_e increases, the beamwidth of the unit cell radiation pattern decreases. Thus, the directivity of the unit cell antenna increases as the value of q_e increases, and the directivity of the unit cell is a function of q_e value. It is apparent that these two expressions show that the aperture efficiency is a function dependent on the reflectarray antenna configuration parameters ($W', L', \theta_0, H, q, q_e$), and this feature can play a crucial role in reflectarray antenna design.

4. PERFORMANCE BOUNDS

The observation is $y = [y_{0,1}, \dots, y_{N-1,T}]^{(T)}$ across all the subcarriers and time in Equation (6). It is assumed that a narrowband signal has $N = 1$ and $T > 1$, which this results in the disappearance of term $e^{-j2\pi n \Delta_f \tau}$, and only $n = 0$ should be considered. Therefore, it would be possible to use different RIS configurations ($\iota = 1, \dots, I$) to make the FIM non-singular. The noise-free term in Equation (7) can be expressed as

$$\Xi = s_0 \mu \sum_{m=1}^M h_m e^{j\omega_{m,\iota}} g_m = s_0 \alpha_{EE_\iota} \quad (26)$$

where $\omega_{m,\iota}$ are the reflectarray antenna weights for different RIS configurations following the UE location displacement. The explicit dependencies of α_{EE_ι} and \mathbf{g} on \mathbf{x} can be inferred. In the next subsection, the performance bounds will be derived.

4.1. Fisher Information and Position Error Bound Analyses

The FIM is composed of the sum of the FIM of each reflectarray antenna m th element and each RIS configuration. The unknowns are $\boldsymbol{\eta} = [\mathbf{x}^T \mid \alpha_{EE_\iota}^T \mid \angle \alpha_{EE_\iota}^T]^T$. The accuracy of FIM primarily depends on taking all variables into account in the estimation. For the sake of brevity, the first two variables are considered in the estimation of FIM for demonstration purpose. The FIM is given by [21] as

$$\mathbf{J}(\boldsymbol{\eta}) = \sum_{\iota=1}^I \sum_{m=1}^M \Re \left\{ \frac{\partial \Xi}{\partial \boldsymbol{\eta}^H} \frac{\partial \Xi}{\partial \boldsymbol{\eta}} \right\} = \sum_{\iota} \sum_m \Re \{ \nabla_{\boldsymbol{\eta}}^H(\Xi) \nabla_{\boldsymbol{\eta}}(\Xi) \}. \quad (27)$$

The non-diagonal entries of the FIM $\mathbf{J}(\mathbf{x}, |\alpha_{EE_\ell}|)$ are equal to zero. Then, by differentiating Ξ with respect to both \mathbf{x} and $|\alpha_{EE_\ell}|$, it yields

$$\begin{aligned}\frac{\partial \Xi}{\partial \mathbf{x}} &= s_0 \alpha_{EE_\ell} \frac{\partial \mathbf{g}}{\partial \mathbf{x}} \\ \frac{\partial \Xi}{\partial |\alpha_{EE_\ell}|} &= s_0 \Im \alpha_{EE_\ell},\end{aligned}\quad (28)$$

where

$$\frac{[\partial \mathbf{g}]_m}{\partial \mathbf{x}} = -jk \frac{\mathbf{x} - \mathbf{q}_m}{|\mathbf{x} - \mathbf{q}_m|} [\mathbf{g}]_m = -jk e_m [\mathbf{g}]_m. \quad (29)$$

e_m is the vector pointing from the m th reflectarray antenna element toward the UE, which leads to

$$\frac{\partial \Xi}{\partial \boldsymbol{\eta}} = s_0 \begin{bmatrix} \alpha_{EE_\ell} \frac{\partial \mathbf{g}}{\partial \mathbf{x}} & \Im \alpha_{EE_\ell} \end{bmatrix}. \quad (30)$$

By substituting Equation (30) into Equation (27), this approximately gives $\mathbf{J}(\boldsymbol{\eta})$. The PEB($\boldsymbol{\eta}$) is then calculated from the resulting $\mathbf{J}(\boldsymbol{\eta})$ and is expressed as in [29]

$$\text{PEB}(\boldsymbol{\eta}) = \sqrt{\text{trace} \mathbf{J}^{-1}(\boldsymbol{\eta})}. \quad (31)$$

The PEB is solely dependent on \mathbf{x} . PEB gives a practical measure of the localization accuracy for near-field communication path established between an offset-fed reflectarray antenna and a single UE.

4.2. RIS Optimal Beamformer

The goal is to control the phases of the radiation sources on the antenna's aperture in such a way that all their contributions sum into an equal phase at a specific location. Therefore, it is important to meet the optimization criterion objective on each antenna m th element of an RIS by satisfying the condition $|\alpha_{EE_\ell}| = 1$. The optimization goal is then formulated into a maximization problem of α_{EE_ℓ} over $\omega_{m,\ell}$, which can be casted into a fitness function expressed as follows

$$\left| \sum_{m=1}^M e^{j\omega_{m,\ell}} e^{-j\psi_{mn}} e^{-jv_{fm}} \right|^2. \quad (32)$$

Therefore, the compensated phases values $\omega_{m,\ell}^*$ have to be adaptively changed to comply with the condition laid down as

$$\omega_{m,\ell}^* = (\psi_{mn} + v_{fm}). \quad (33)$$

Clearly, the optimization goal is to find $\boldsymbol{\Omega}$, which provides the best positioning quality for the UE. The optimization fitness function solely depends on the delay measurements. A proper choice of $\omega_{m,\ell}^*$ values would result in finely focusing the scattered field at the target area. It is worth to mention that the optimal RIS beamformer can be realized as well by reconfigurable metasurfaces, which are usually embedded onto the walls in the smart radio environments as discussed in [30–33].

5. NUMERICAL RESULTS

5.1. Simulation Specification

An OFDM system operates at $f_c = 2.4$ GHz with total bandwidth $W = 312.5$ kHz, using 1-subcarrier and QPSK pilot. The transmitting power is set to 1 mW. The RIS consists of a reflectarray antenna of $M = 144$ unit cells, extending from $[-0.4, -0.4]$ to $[0.4, 0.4]$ m in x - y plane with an interelement spacings $\Delta x = \Delta y = 6.25$ cm in both the x and y coordinates. The reflectarray antenna unit cells dimensions are tabulated in [27]. The unit cells of the reflectarray antenna are realized by using microstrip patches. The structure of the reflectarray antenna unit cell, constituent materials, and their electrical properties such as relative permittivity ϵ_r and loss tangent $\tan \delta$, and thickness are shown in Figure 3. Their phases $\omega_{m,\ell}$ are implemented by changing the sizes of the patches, which compensates the spatial phase delays

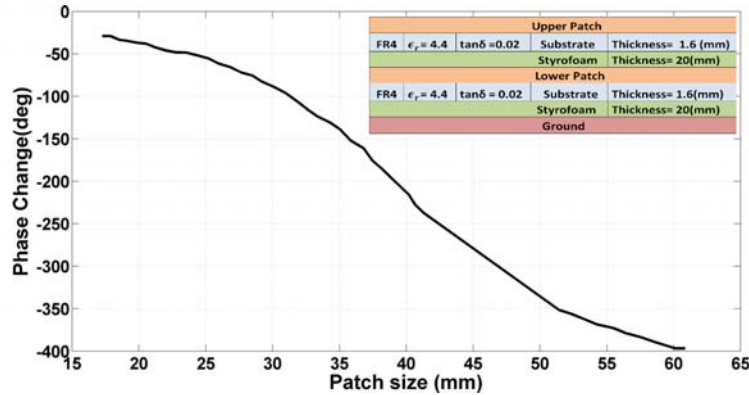


Figure 3. The structure of the reflectarray unit cell and its phase variations versus the patch size, reproduced from [27].

of the scattered fields. The operating principle of the variable size technique is based on the fact that the reflected phase from resonant unit cells with different sizes would be different [22]. The reflectarray unit cell and its phase variation curve versus the patch size are reproduced from [27] for illustration purpose. The overall structure of the reflectarray antenna is depicted in Figure 1. The feed antenna is located at an altitude of $H = 0.351$ m and creates an offset angle $\theta_0 = 26^\circ$ from the reflectarray antenna aperture. The radiation pattern model of the feed antenna is assumed to have an exponent of $q = 2.0$, and the radiation pattern for the unit cells is modeled with an exponent of $q_e = 2.5$ irrespective of their varying patch sizes for simplicity purpose. The design goal is to have a target focus area of 0.5×0.5 m² at a distance 0.9 m away from the reflectarray antenna aperture along the propagation path \hat{r} .

5.2. Results and Discussion

The radiation patterns of only scattered fields on different coordinate systems $u-r$, $r-V$, and $u-V$ are displayed, whilst the fields directly radiated from the feed antenna are neglected. The definition of $u-V-r$ coordinate systems is illustrated in Figure 2(a). The plane $\hat{u}-\hat{V}$ is on the cross section orthogonal to the propagation path; meanwhile, the $\hat{u}-\hat{r}$ plane is along the propagation path to display the characteristics of scattered fields. To validate the near-field model, the simulation results are compared to the simulation ones of the model discussed in literature work in [19] using Matlab software. It is considered that $d_0 = 2$ m, which results in an appearance of the peak value of the field at $r = 0.9$ m along the propagation

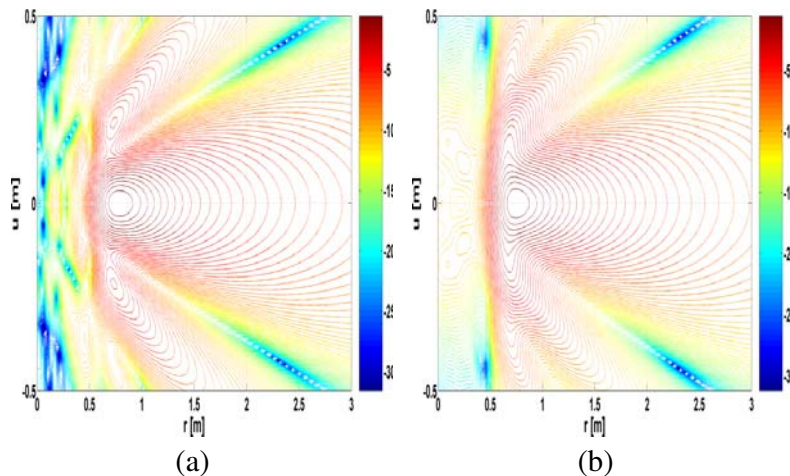


Figure 4. Contoured radiation patterns on the $\hat{u}-\hat{r}$ plane in the near-zone. The results were obtained by using (a) the developed model versus (b) the model discussed in literature.

path. This exactly meets the design requirements of having a target focus area at the same distance. The spillover and illumination efficiencies are computed using Equations (24) and (25), respectively. The aperture efficiency is the product of these two terms, and it corresponds to 73%.

Figure 4 shows contoured radiation patterns of the developed near-field model and the model discussed in literature on the plane $u-r$ along the propagation path. A good agreement is shown between the simulation results. Due to the symmetry of the reflectarray antenna structure along the y -axis, the location of the peak field strength appears on the $y-z$ plane. The field distribution along the propagation path exhibits the field peak at around $r = 0.9$ m. The contoured radiation pattern along the propagation path in Figure 5 is taken along the r -axis on $r-V$ plane. It also shows good field distribution within the desired target area, whereas the fields outside the target area are tapered down to lower levels. This conforms with the developed model limitation of having a uniform phase distribution on the reflectarray antenna aperture.

The contoured radiation pattern is displayed in Figure 6 on the $u-V$ coordinate at a distance $r = 90$ cm. It exhibits the field focusing properties before and after the field strength peak occurs. This shows a target focus area of roughly 0.5×0.5 m², which fulfills the design goal. To better visualize

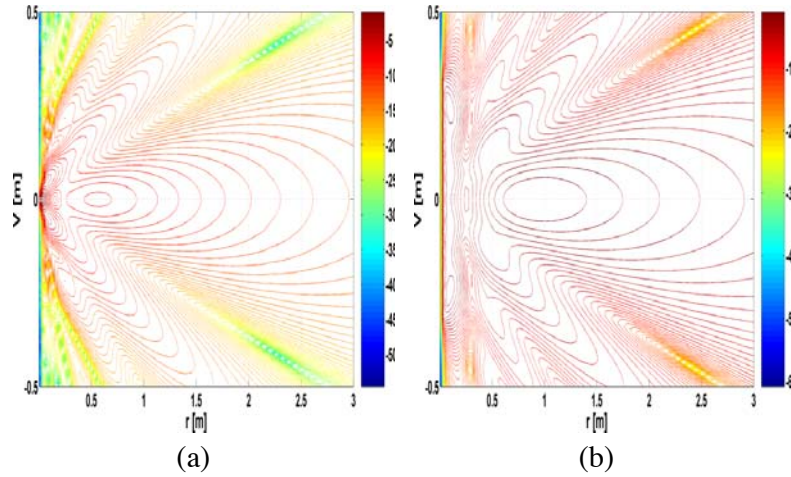


Figure 5. Contoured radiation patterns on the $\hat{r}-\hat{V}$ plane in the near-zone. The results were obtained by using (a) the developed model versus (b) the literature discussed in literature.

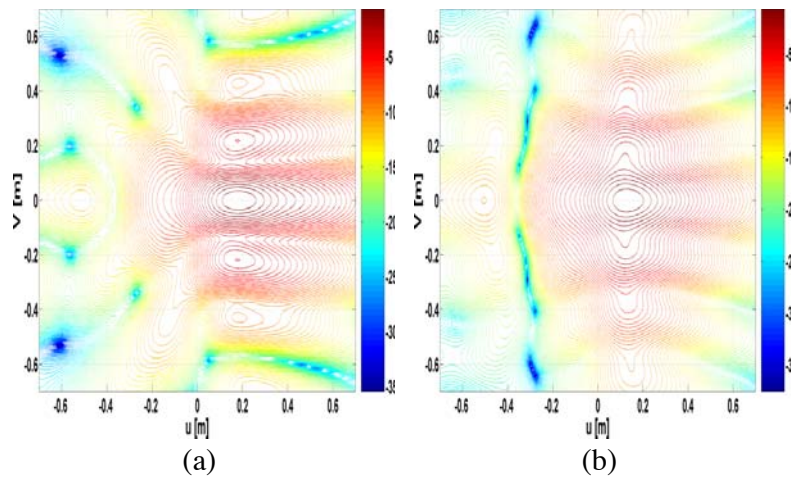


Figure 6. Contoured radiation patterns on the $\hat{u}-\hat{V}$ plane in the near-zone. The results were obtained by using (a) the developed model versus (b) the model discussed in literature.

the focus area, it is demonstrated that the radiation pattern starts to focus with an increasing power density right after the fields scattered by the reflectarray antenna aperture reaching its maximum value, then the radiation pattern becomes de-focused as depicted in Figures 4 and 5. Thus, this region can be marked as the focusing region for practical applications.

Figure 7(a) shows the phase distribution in radians on the reflectarray antenna aperture for the case of the optimal RIS focusing the beam into the target area. The phase distribution values reach several times of 360° , which is practically realized by using multilayer elements to achieve a smoother-linear behavior of the phase as a function of the dimensions of the patches. This phase distribution can be further used for deployment of the reflectarray antenna mask. The spatial distribution of the PEB for the optimal RIS is shown in Figure 7(b), where the PEB takes on lower values closer to the focal point. In the region surrounding the target focus area, lower PEB values can still be achieved throughout this region for the case of an optimized RIS.

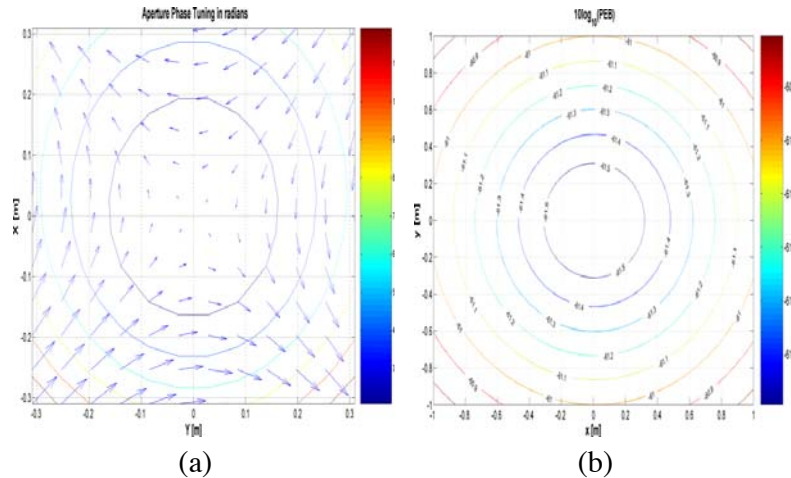


Figure 7. (a) RIS optimal beamformer phase distribution implemented by changing the reflectarray antenna unit cells dimensions for beam focusing at the target area, (b) PEB as a function of the user location, and the RIS acts as an optimal beamformer.

Finally, the reflectarray antenna is thinned with the goal of having an equal focus area size with much fewer unit cells than the case of fully populated reflectarray antenna elements ($M = 144$). For the case of nonuniform reflectarray antenna elements, it usually contains a large pool of variables to be processed by the optimization algorithm [34]. Alternatively, the removal of clustered elements in small groups of 2×1 elements offers a good option for thinning at a low complexity as in [35]. The removal criteria of clustered elements take into consideration many factors, to name a few: conformity the symmetry of the reflectarray antenna configuration and the phases distribution of an offset fed-antenna on the reflectarray antenna aperture. The locations of the unit cells close to the reflectarray antenna center are then optimized by maximizing the magnitude of the electric field distribution onto a focus area plane at $r = 0.9$ m.

The objective function involves the maximization of the magnitude of the electric field on a size-limited focus region on xy -plane close to the reflectarray antenna aperture. Therefore, the problem is a typical optimization problem with a limited degree of freedom represented by the locations of the unit cells close to the reflectarray antenna center. The constraints are imposed by the requirement of avoiding the mutual coupling effect, which necessitates a minimum $\lambda/2$ separation guard distance between adjacent unit cells. A cost function establishes the maximum field bounds for different points in the targeted focus near-field region, and a proper stopping criterion sets to account for the minimization of the error difference. The genetic algorithm (GA) has been programmed in CST MWS for achieving this fitness function. The simulation results of the optimum thinned reflectarray antenna depicted in in Figure 8 show a good agreement with the exact reflectarray antenna and fulfill the target focused area requirement with a reduction factor up to (6%).

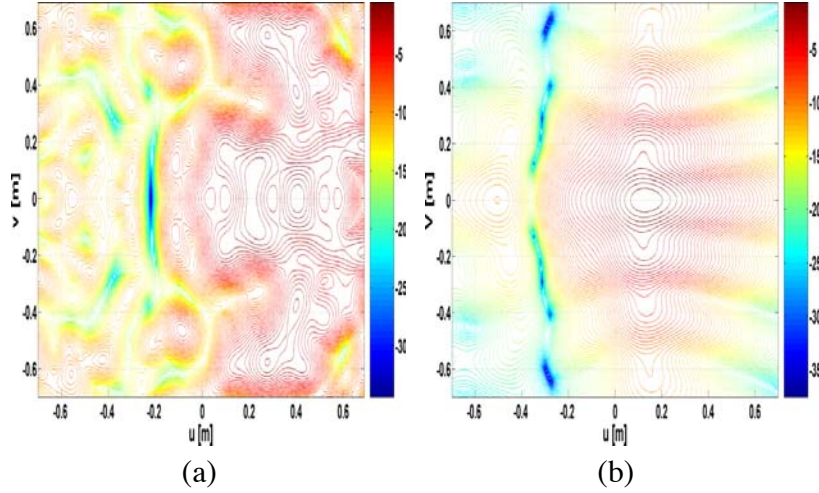


Figure 8. (a) Contoured radiation patterns on the \hat{u} - \hat{V} plane obtained by using the thinned array versus (b) the model discussed in literature.

To verify and validate the developed near-field model, recall that the gain has to be maximum at the focal point [23]. Thus, the normalized gain is computed using the developed near-field model and the model described in the literature [19]. The simulation result depicted in Figure 9(a) satisfies the focus condition, and it also complies with the simulation result shown in Figure 9(b). Since the focal point is located away from the boresight direction, the sidelobes are visible close to the focus zone.

A comparison between simulated scattered fields along the propagation path r is performed off the reflectarray aperture. It shows that the field peaks coincide at nearly $r = 0.9$ m. Figure 10(a) shows the normalized field and -3 dB beamwidths along the propagation path. A good agreement is found for peak field locations and range of -3 dB beamwidths. Figure 10(b) displays the derivatives of the power densities along the propagation path. It is clear that the maximum field strengths appearing in Figure 10(a) coincide at the locations where the derivatives are equal to zero in Figure 10(b).

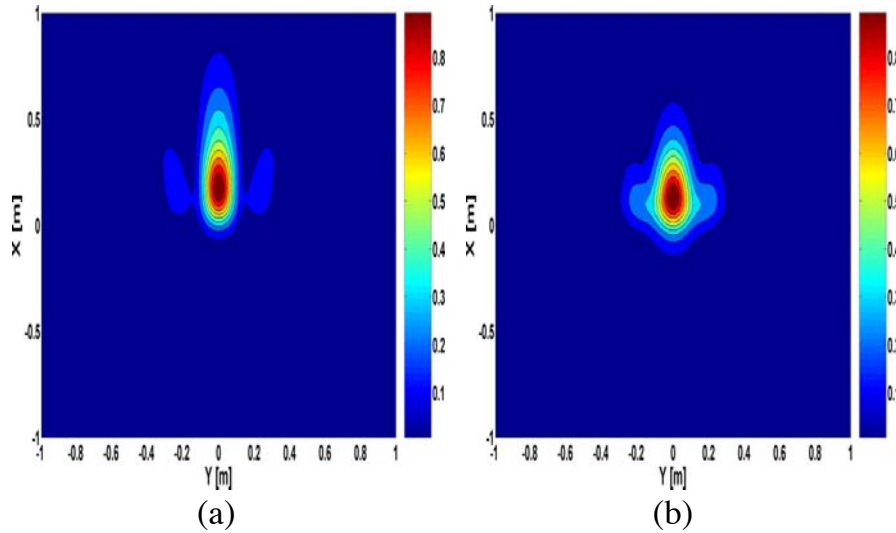


Figure 9. Contoured normalized gain on the x - y plane along the propagation path r obtained by (a) the developed near-field model, (b) the model discussed in literature.

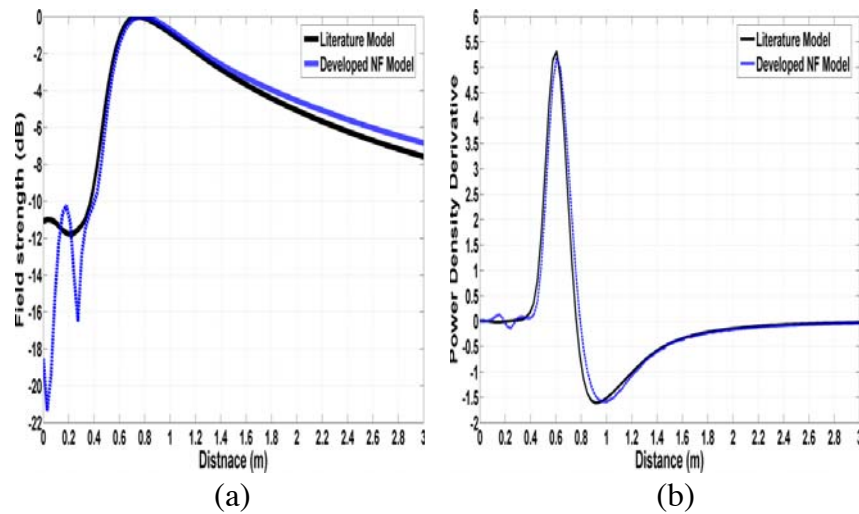


Figure 10. (a) Normalized scattered fields in (dB) and -3 dB beamwidths of model discussed in the literature and developed near-field model along the propagation path r , (b) derivative of the power density of both models.

6. CONCLUSION

A near-field channel gain model has been developed for NFF RISs. The channel gain model exhibits different features, i.e., low complexity burden which is a prevalent requirement for changing environment. Reflectarray reconfigurability is also considered in evaluating the channel gain, and the channel gain efficiency is derived from the configuration of an offset-fed reflectarray antenna. The positioning performance bounds FIM and PEB benefit from the developed model in computing positioning bounds. The simulation results of the developed model are validated with results presented in literature, and the simulation results show good agreement. As future developments, different phase tuning methods for synthesizing aperture phase distribution will be explored with the aim of modifying this near-field channel gain model.

ACKNOWLEDGMENT

The author would like to thank Prof. Henk Wymeersch for technical discussions on the topic of RIS and localization.

REFERENCES

1. Di Renzo, M., A. Zappone, M. Debbah, M. S. Alouini, C. Yuen, J. de Rosny, and S. Tretyakov, "Smart radio environments empowered by reconfigurable intelligent surfaces: How it works, state of research, and the road ahead," *IEEE Journal on Selected Areas in Communications*, Vol. 38, No. 11, 2450–2525, 2020.
2. ElMossallamy, M. A., H. Zhang, L. Song, K. G. Seddik, Z. Han, and G. Y. Li, "Reconfigurable intelligent surfaces for wireless communications: Principles, challenges, and opportunities," *IEEE Transactions on Cognitive Communications and Networking*, Vol. 6, No. 3, 990–1002, 2020.
3. Liaskos, C., A. Tsioliariidou, A. Pitsillides, S. Ioannidis, and I. F. Akyildiz, "Using any surface to realize a new paradigm for wireless communications," *ACM Commun.*, Vol. 61, No. 11, 30–33, Nov. 2018.

4. "The next hyper — Connected experience for all," White Paper, Samsung 6G Vision, Jun. 2020.
5. Pan, C., H. Ren, K. Wang, M. Elkashlan, A. Nallanathan, J. Wang, and L. Hanzo, "Intelligent reflecting surface aided mimo broadcasting for simultaneous wireless information and power transfer," *IEEE Journal on Selected Areas in Communications*, 2020.
6. Chu, Z., W. Hao, P. Xiao, and J. Shi, "Intelligent reflecting surface aided multi-antenna secure transmission," *IEEE Wireless Communications Letters*, Vol. 9, No. 1, 108–112, 2019.
7. Park, S. Y. and D. I. Kim, "Intelligent reflecting surface-aided phaseshift backscatter communication," *2020 14th International Conference on Ubiquitous Information Management and Communication (IMCOM)*, 1–5, IEEE, 2020.
8. Zhang, H., H. Zhang, B. Di, K. Bian, Z. Han, and L. Song, "Towards ubiquitous positioning by leveraging reconfigurable intelligent surface," *IEEE Communications Letters*, Sep. 10, 2020.
9. Nepa, P. and A. Buffi, "Near-field-focused microwave antennas: Near-field shaping and implementation," *IEEE Antennas and Propagation Magazine*, Vol. 59, No. 3, 42–53, 2017.
10. Huang, C., G. C. Alexandropoulos, C. Yuen, and M. Debbah, "Indoor signal focusing with deep learning designed reconfigurable intelligent surfaces," *2019 IEEE 20th International Workshop on Signal Processing Advances in Wireless Communications (SPAWC)*, 1–5, 2019.
11. Nayeri, P., A. Z. Elsherbeni, R. L. Haupt, and F. Yang, "Near-field scanning characteristics of focused reflectarray antennas," *2015 31st International Review of Progress in Applied Computational Electromagnetics (ACES)*, 1–2, IEEE, 2015.
12. Dehnavi, M. M. and J. Laurin, "Near field focusing using a circularly polarized reconfigurable reflectarray," *2019 IEEE International Symposium on Antennas and Propagation and USNC-URSI Radio Science Meeting*, 1953–1954, 2019.
13. Di Renzo, M., F. Habibi Danufane, X. Xi, J. de Rosny, and S. Tretyakov, "Analytical modeling of the path-loss for reconfigurable intelligent surfaces — Anomalous mirror or scatterer?," *2020 IEEE 21st International Workshop on Signal Processing Advances in Wireless Communications (SPAWC)*, 1–5, 2020.
14. Tang, W., M. Z. Chen, X. Chen, J. Y. Dai, Y. Han, M. Di Renzo, Y. Zeng, S. Jin, Q. Cheng, and T. J. Cui, "Wireless communications with reconfigurable intelligent surface: Path loss modeling and experimental measurement," *IEEE Transactions on Wireless Communications*, 2020.
15. Hu, S., F. Rusek and O. Edfors, "The potential of using large antenna arrays on intelligent surfaces," *2017 IEEE 85th Vehicular Technology Conference (VTC Spring)*, 1–6, Sydney, NSW, 2017, doi: 10.1109/VTCspring.2017.8108330.
16. Garcia, J. C. B., A. Sibille, and M. Kamoun, "Reconfigurable intelligent surfaces: Bridging the gap between scattering and reflection," *IEEE Journal on Selected Areas in Communications*, Vol. 38, No. 11, 2538–2547, 2020.
17. Tuan, S. and H. Chou, "Asymptotic analysis of scattering from reflectarray antennas for the near-field focused applications," *2015 Asia-Pacific Symposium on Electromagnetic Compatibility (APEMC)*, 173–176, 2015.
18. Arrebola, M., Y. Alvarez, J. A. Encinar, and F. Las-Heras, "Accurate analysis of printed reflectarrays considering the near field of the primary feed," *IET Microwaves, Antennas Propagation*, Vol. 3, No. 2, 187–194, 2009.
19. Chou, H., T. Hung, N. Wang, H. Chou, C. Tung, and P. Nepa, "Design of a near-field focused reflectarray antenna for 2.4 GHz rfid reader applications," *IEEE Transactions on Antennas and Propagation*, Vol. 59, No. 3, 1013–1018, 2011.
20. Hu, S., F. Rusek, and O. Edfors, "Beyond massive MIMO: The potential of positioning with large intelligent surfaces," *IEEE Trans. Signal Process.*, Vol. 66, No. 7, 1761–1774, Apr. 2018.
21. Wymeersch, H. and B. Denis, "Beyond 5G wireless localization with reconfigurable intelligent surfaces," *Proc. IEEE ICC*, 1–6, Dublin, Ireland, Jun. 2020.
22. Huang, J. and J. A. Encinar, *Antenna Analysis Techniques*, Chapter 3, 27–78, John Wiley & Sons, Ltd, 2007, [online], available: <https://onlinelibrary.wiley.com/doi/abs/10.1002/9780470178775.ch3>.

23. Sherman, J., "Properties of focused apertures in the fresnel region," *IRE Transactions on Antennas and Propagation*, Vol. 10, No. 4, 399–408, 1962.
24. Silver, S., *Microwave Antenna Theory and Design*, Massachusetts Institute of Technology, Radiation Laboratory Series, No. 12, McGraw-Hill Book Company, 1949, [online], available: <https://books.google.com.eg/books?id=Fi42MwEACAAJ>.
25. Nayeri, P., et al., *System Design and Aperture Efficiency Analysis*, Chapter 3, 49–78, John Wiley & Sons, Ltd, 2018, [online], available: <https://onlinelibrary.wiley.com/doi/abs/10.1002/9781118846728.ch3>.
26. Mielenz, K. D., "Computation of fresnel integrals. II." *Journal of Research of the National Institute of Standards and Technology*, Vol. 105, No. 4, 589–590, 2000.
27. Chou, H., Y. Liu, X. Dong, B. You, and L. Kuo, "Design of reflectarray antennas to achieve an optimum near-field radiation for RFID applications via the implementation of SDM procedure," *Radio Science*, Vol. 50, No. 4, 283–293, 2015.
28. Nayeri, P., F. Yang, and A. Z. Elsherbeni, *System Design and Aperture Efficiency Analysis*, 49–78, 2018.
29. He, J., H. Wymeersch, L. Kong, O. Silv'en, and M. Juntti, "Large intelligent surface for positioning in millimeter wave MIMO systems," *Proc. IEEE VTC-Spring*, 1–5, Antwerp, Belgium, May 2020.
30. Basar, E., M. Di Renzo, J. De Rosny, M. Debbah, M. Alouini, and R. Zhang, "Wireless communications through reconfigurable intelligent surfaces," *IEEE Access*, Vol. 7, 116 753–116 773, 2019.
31. Di Renzo, M., M. Debbah, D.-T. Phan-Huy, A. Zappone, M.-S. Alouini, C. Yuen, V. Sciancalepore, G. C. Alexandropoulos, J. Hoydis, H. Gacanin, J. de Rosny, A. Bounceur, G. Lerosey, and M. Fink, "Smart radio environments empowered by reconfigurable AI meta-surfaces: An idea whose time has come," *EURASIP J. Wireless Commun. Netw.*, Vol. 2019, No. 1, 1–20, May 2019.
32. Liaskos, C., S. Nie, A. Tsioliariidou, A. Pitsillides, S. Ioannidis, and I. Akyildiz, "A new wireless communication paradigm through softwarecontrolled metasurfaces," *IEEE Communications Magazine*, Vol. 56, No. 9, 162–169, 2018.
33. Zhang, H., J. Hu, H. Zhang, B. Di, K. Bian, Z. Han, and L. Song, "Metaradar: Indoor localization by reconfigurable metamaterials," *IEEE Transactions on Mobile Computing*, Dec. 14, 2020.
34. Johnson, J. M. and V. Rahmat-Samii, "Genetic algorithms in engineering electromagnetics," *IEEE Antennas and Propagation Magazine*, Vol. 39, No. 4, 7–21, 1997.
35. Ulichny, K., E. Levine, and H. Matzner, "Design of thinned antenna arrays," *2015 IEEE 5th Asia-Pacific Conference on Synthetic Aperture Radar (APSAR)*, 238–241, 2015.